Photonic band-gap formation by optical-phase-mask lithography

Timothy Y. M. Chan, Ovidiu Toader, and Sajeev John
Department of Physics, University of Toronto, 60 St. George Street, Toronto, Ontario, M5S 1A7, Canada
(Received 2 November 2005; published 26 April 2006)

We demonstrate an approach for fabricating photonic crystals with large three-dimensional photonic band gaps (PBG's) using single-exposure, single-beam, optical interference lithography based on diffraction of light through an optical phase mask. The optical phase mask (OPM) consists of two orthogonally oriented binary gratings joined by a thin, solid layer of homogeneous material. Illuminating the phase mask with a normally incident beam produces a five-beam diffraction pattern which can be used to expose a suitable photoresist and produce a photonic crystal template. Optical-phase-mask Lithography (OPML) is a major simplification from the previously considered multibeam holographic lithography of photonic crystals. The diffracted five-beam intensity pattern exhibits isointensity surfaces corresponding to a diamondlike (face-centered-cubic) structure, with high intensity contrast. When the isointensity surfaces in the interference patterns define a silicon-air boundary in the resulting photonic crystal, with dielectric contrast 11.9 to 1, the optimized PBG is approximately 24% of the gap center frequency. The ideal index contrast for the OPM is in the range of 1.7–2.3. Below this range, the intensity contrast of the diffraction pattern becomes too weak. Above this range, the diffraction pattern may become too sensitive to structural imperfections of the OPM. When combined with recently demonstrated polymer-to-silicon replication methods, OPML provides a highly efficient approach, of unprecedented simplicity, for the mass production of large-scale three-dimensional photonic band-gap materials.

DOI: 10.1103/PhysRevE.73.046610 PACS number(s): 42.70.Qs

I. INTRODUCTION

Photonic band-gap (PBG) materials [1,2] are periodically ordered dielectric microstructures which forbid electromagnetic waves of a certain spectral region from propagating in the crystal. The most profound properties of these artificial materials arise from their ability to trap or localize light [3]. These photonic crystals provide a robust platform for integrating active and passive devices in an all-optical microchip [4]. In order to realize an optical microchip, capable of localizing and micromanipulating light, it is necessary to have high-quality, three-dimensional (3D) PBG materials. Efficient, large-scale microfabrication of PBG materials, with high accuracy and low cost, has been a major scientific and technological challenge over the past decade. The difficulties in large-scale microfabrication of 3D architectures have led to extensive studies of alternative 2D photonic crystal membrane architectures. While 2D photonic crystals are more amenable to conventional methods of semiconductor microlithography, they lack the most profound properties of the photonic band gap: namely, complete localization of light and control over the electromagnetic density of states. In this paper, we suggest that the large-scale microfabrication of 3D photonic band-gap materials is considerably simplified using optical-phase-mask lithography (OPML). We describe the design of optical phase masks (OPM's) that reduce the task of large-scale and repetitive synthesis of PBG materials, with photonic band gaps as large as 24% relative to center frequency, to two simpler tasks. The first is the illumination (single exposure) of a photoresist material with a single laser beam at normal incidence to the phase mask and sample surface. The second is the replication of the "developed" photoresist with a high-refractive-index semiconductor, such as silicon, using previously established methods [5].

The diamond lattice structure has been shown theoretically [6] to be the quintessential architecture for creation of a large 3D PBG. This discovery has spurred several theoretical blueprints and subsequent fabrication attempts for photonic crystals based on "diamondlike" structures employing nonspherical bases on an fcc lattice. One diamondlike architecture is the layer-by-layer "woodpile" structure comprised of stacked two-dimensional photonic crystals [7,8], which can have a PBG approximately 18% of the gap center frequency. Techniques such as repetitive deposition and etching of silicon [9,10], wafer-fusion and laser-assisted alignment [11], and nanofabrication of the two-dimensional layers followed by microassembly of the layers [12] have been used to produce high-quality woodpile structures with PBG's in the optical regime. Unfortunately, these samples are only a few periods deep in the stacking direction. Recently, "direct laser writing" processes involving two-photon absorption (causing polymerization) in resins have been used to produce woodpile structures as a proof of concept [13–15]. An alternative approach towards fabricating diamondlike structures uses glancing-angle deposition methods [16] to form silicon square spiral posts on a silicon substrate. A PBG as large as 24% of the gap center frequency has been predicted for suitably architectured spiral structures [17,18]. Optical reflectivity in a weakly disordered version of these silicon square spiral crystals has revealed a 3D PBG of roughly 10% relative to the center frequency [19]. An fcc lattice of crisscrossing pores is another diamondlike architecture which has been shown to exhibit a 3D PBG [20]. Attempts to fabricate this structure on a submicron-scale have included electron beam lithography followed by reactive ion etching [21,22], deep x-ray lithography (LIGA) patterning of an x-ray sensitive resist [23], and photoelectrochemical etching followed by focused-ion-beam etching [24]. However, the first method produced only a few periods of the structure, with severe imperfections at the pore crossing points, while samples created by the latter two methods have had feature sizes too

large for a PBG in the optical regime. Recently, new "slanted pore" architectures have been introduced [25] whose simpler geometries may facilitate their fabrication by various pore etching methods. Another approach towards the fabrication of 3D photonic crystals relies on the colloidal self-assembly of silica spheres into an fcc opal lattice. The silica spheres are used as a template which is inverted by chemical vapor deposition of silicon, followed by selective etching of the silica template [26–28], in a process which can be performed at large scales. In contrast to the approaches already mentioned, this "inverse opal" architecture cannot be characterized as diamondlike, and as a result, the PBG is only 9% of the gap center frequency [29] and vulnerable to disorder [30], necessitating that the fabrication methods yield very-high-quality structures.

Recently, the holographic lithography method [31–33] has been suggested as an alternative approach to large-scale synthesis of 3D photonic crystals with large PBG's in the optical regime. In this approach, a 3D intensity pattern formed by the interference of four or more laser beams exposes a photopolymerizable material such as a photoresist. The photoresist undergoes a chemical alteration when the total light intensity at position $\vec{r}$ due to the interference pattern, $I(\vec{r})$, is maintained over a time $\delta\tau$ such that the "exposure" $I(\vec{r})\delta\tau$ exceeds a specified threshold T. For negative photoresists, the "underexposed" regions can then be selectively removed using a developer substance which leaves the "overexposed" regions intact. (For positive photoresists, the overexposed regions are removed and the underexposed regions remain after developing.) The developed material can then be infiltrated at room temperature with SiO_2 [34] and burned away, leaving behind a daughter "inverse" template. Finally, the daughter template is inverted by high-temperature infiltration with silicon [27,35] and selective chemical etching of the SiO_2. As a result, a 3D silicon photonic crystal is formed, in which the silicon-air boundary is defined by the original, optical isointensity surface $I(\vec{r})\delta\tau=T$. Most previous theoretical reports have discussed the formation of 3D photonic crystals by holographic lithography based on single exposure of the photoresist by the interference pattern of four laser beams. It has been shown [36–39] that using configurations of this form, it is possible to produce a diamondlike structure with a PBG approximately 25% of the center frequency when synthesized with a material with a dielectric constant of 11.9, corresponding to Si. Despite the promise of multibeam interference lithography, the precise alignment of four laser beams from different directions is experimentally inconvenient. Restricting all four beams to be launched from the same half-space (umbrella setup) reduces the PBG significantly [40,41].

In this paper, we circumvent these complications and drawbacks using an interference pattern generated by a single beam diffracting through a carefully designed phase mask [42]. The use of diffractive interference patterns from phase masks has previously been shown to produce diamondlike photonic crystals provided that two independent optical exposures are performed with two separate positions of the phase mask [43]. However, realignment of the second exposure with the first exposure is a daunting experimental challenge. Simple fcc structures that do not lead to a large PBG can be achieved with a single exposure [44]. Here, we introduce a novel approach to create a diamondlike structure by OPML based on single exposure of a photoresist by a laser beam leading to a five-beam interference pattern. We present a phase mask design that yields a diamondlike structure with a PBG of 24% of the gap center frequency when synthesized with a material with a dielectric constant of 11.9. In Sec. II we introduce the target five-beam intensity pattern and its relation to the intensity pattern emerging from the diffraction of a single beam through an OPM. In Sec. III, we describe the proposed OPM architecture. In Sec. IV we show several phase mask geometries that can produce photonic crystals with large PBG's and we study the effects on the resulting PBG when the phase mask parameters are varied and the polarization of the incident beam is varied. In particular, we find that when the photoresist has a refractive index corresponding to 1.67 (undeveloped SU-8 at 355-nm wavelength [45]), the ideal index contrast for the OPM is in the range of 1.7–2.3.

II. DIFFRACTION OF LIGHT BY OPTICAL PHASE MASKS

Consider a single, monochromatic beam with vacuum wavelength λ_0 and wave vector $\vec{k}_0=-2\pi/\lambda_0\hat{z}$, normally incident onto an optical phase mask and exposing a region with refractive index $n^{(-)}$ below the mask. The phase mask is assumed to have a square Bravais lattice symmetry, with lattice constant a, finite thickness in the z direction, and mirror planes normal to $\hat{x}$ and $\hat{y}$. For a uniform incident beam with infinite extent in the x and y directions, the electric field in the exposure region consists of the unscattered beam with wave vector $\vec{G}_{00}=-2\pi n^{(-)}/\lambda_0\hat{z}$ and diffracted beams with wave-vectors $\vec{G}_{mn}=2\pi/a(m,n,-\gamma_{mn})$, where m and n are arbitrary integers. These diffracted beams have wave-vector components in the xy plane, $2\pi/a(m,n,0)$, corresponding to the Fourier components of the OPM dielectric profile. The z component of the wave vector of mode (m,n) is determined by the condition of energy conservation $|\vec{k}_0|=|\vec{G}_{mn}|/n^{(-)}$:

$$\gamma_{mn}=\pm[\alpha^2-m^2-n^2]^{1/2},\quad \alpha\equiv an^{(-)}/\lambda_0. \tag{1}$$

In general, γ_{mn} can be a complex number, describing either propagating or evanescent beams in the region of the photoresist ($z<0$). From earlier studies of multibeam optical interference lithography [38,46], it is desireable to have five and only five propagating modes in the exposure region: namely, the $(0,0)$, $(0,\pm1)$, and $(\pm1,0)$ modes, with corresponding wave vectors

$$\vec{G}_{00}=\frac{2\pi}{a}(0,0,-q_0),\quad \vec{G}_{ij}=\frac{2\pi}{a}(i,j,-q_1), \tag{2}$$

where $\bar{i}\equiv-i$ and $\bar{j}\equiv-j$. Here we have defined

$$q_j\equiv\sqrt{\alpha^2-j}. \tag{3}$$

In order for these modes to propagate in the exposure region, we require $(an^{(-)}/\lambda_0)^2>1$, or $\lambda_0/a<n^{(-)}$. The next lowest-order modes are the $(\pm1,\pm1)$ modes, which have wave vec-

tors of the form $\vec{G}_{\langle 11\rangle}=2\pi/a(\pm 1,\pm 1,-q_2)$. For these (and all higher-order) modes to be evanescent in the exposure region, we require $(an^{(-)}/\lambda_0)^2<2$, or $\lambda_0/a>n^{(-)}/\sqrt{2}$. Therefore, in order to retain only the desired modes, the incident beam wavelength is constrained by

$$n^{(-)}/\sqrt{2}<\lambda_0/a<n^{(-)}. \tag{4}$$

Provided that the constraint in Eq. (4) is satisfied, then an intensity pattern is produced corresponding to the interference pattern of five monochromatic plane waves of frequency ω, wave vectors $\vec{G}_l$ corresponding to Eq. (2), polarization vectors $\vec{E}_l$, and phases θ_l, where l is in the set $\mathcal{L}=\{00,10,\bar{1}0,01,0\bar{1}\}$. The electric field associated with this interference pattern is given by

$$\vec{E}(\vec{r},t)=e^{-i\omega t}e^{i(\vec{G}_{00}\cdot\vec{r}+\theta_{00})}\left[\vec{E}_{00}+\sum_{l\neq 00}\vec{E}_l e^{i(\vec{K}_l\cdot\vec{r}+\varphi_l)}\right], \tag{5}$$

where $\vec{K}_l$ and φ_l are defined as

$$\vec{K}_l\equiv\vec{G}_l-\vec{G}_{00},$$

$$\varphi_l\equiv\theta_l-\theta_{00}. \tag{6}$$

The corresponding intensity pattern is given by

$$I(\vec{r})=I_0+2\sum_{l\neq 00}\eta_{00\cdot l}\cos[\vec{K}_l\cdot\vec{r}+\tau_{00\cdot l}+\varphi_l]+2\sum_{l\neq 00}\sum_{l'>l}\eta_{l'\cdot l}\cos[(\vec{K}_l-\vec{K}_{l'})\cdot\vec{r}+\tau_{l'\cdot l}+\varphi_l-\varphi_{l'}], \tag{7}$$

where

$$I_0\equiv\sum_l|\vec{E}_l|^2 \tag{8}$$

and

$$\eta_{l'\cdot l}\equiv|\vec{E}^*_{l'}\cdot\vec{E}_l|,$$

$$\tau_{l'\cdot l}\equiv\arg(\vec{E}^*_{l'}\cdot\vec{E}_l). \tag{9}$$

The spatial modulation of this intensity pattern is periodic with a Bravais lattice whose reciprocal lattice vectors can be represented by any three vectors from the set $\mathcal{K}=\{\vec{K}_{10},\vec{K}_{\bar{1}0},\vec{K}_{01},\vec{K}_{0\bar{1}}\}$:

$$\vec{K}_{ij}=\left(\frac{2\pi i}{a},\frac{2\pi j}{a},\frac{2\pi}{c}\right), \tag{10}$$

where $\bar{i}\equiv -i$ and $\bar{j}\equiv -j$. Here we have defined

$$c\equiv a[q_0-q_1]^{-1}=a[\alpha-\sqrt{\alpha^2-1}]^{-1}. \tag{11}$$

It is easy to verify that the fourth vector from $\mathcal{K}$ can then be written as a linear combination, with integral coefficients, of the other three vectors in the set. This reveals that the five-beam intensity pattern resulting from diffraction of light through the OPM has tetragonal Bravais lattice symmetry, with aspect ratio c/a.

The form of the intensity pattern can be simplified by symmetry arguments. For a normally incident beam and a phase mask with reflection symmetry in both x and y, as considered here, the electric-field components and phases satisfy the following symmetries:

$$E^x_{10}=E^x_{\bar{1}0},\quad E^y_{10}=E^y_{\bar{1}0},\quad E^z_{10}=-E^z_{\bar{1}0},$$

$$E^x_{01}=E^x_{0\bar{1}},\quad E^y_{01}=E^y_{0\bar{1}},\quad E^z_{01}=-E^z_{0\bar{1}},$$

$$\varphi_{10}=-\varphi_{\bar{1}0},\quad \varphi_{01}=-\varphi_{0\bar{1}}. \tag{12}$$

The relations involving the phases φ imply that they can be eliminated by a translation of the origin, $\vec{r}\rightarrow\vec{r}-\vec{\delta}_1$, where $\vec{\delta}_1=a/2\pi(\varphi_{10},\varphi_{01},0)$. Using the fact that the unscattered (central) beam is transverse ($E^z_{00}=0$), the relations (12) involving the **E**-field components imply that

$$\eta_{00\cdot 10}=\eta_{00\cdot\bar{1}0}\equiv c_1,\quad \tau_{00\cdot 10}=\tau_{00\cdot\bar{1}0}\equiv\phi_1,$$

$$\eta_{00\cdot 01}=\eta_{00\cdot 0\bar{1}}\equiv c_2,\quad \tau_{00\cdot 01}=\tau_{00\cdot 0\bar{1}}\equiv\phi_2,$$

$$\eta_{10\cdot 01}=\eta_{\bar{1}0\cdot 0\bar{1}}\equiv c_3,\quad \tau_{10\cdot 01}=\tau_{\bar{1}0\cdot 0\bar{1}}\equiv\phi_3,$$

$$\eta_{10\cdot 0\bar{1}}=\eta_{\bar{1}0\cdot 01}\equiv c_4,\quad \tau_{10\cdot 0\bar{1}}=\tau_{\bar{1}0\cdot 01}\equiv\phi_4. \tag{13}$$

Here the relations involving ϕ_i are modulo 2π. Defining $c_5\equiv\eta_{\bar{1}0\cdot 10}$, $\phi_5\equiv\tau_{\bar{1}0\cdot 10}$, $c_6\equiv\eta_{0\bar{1}\cdot 01}$, and $\phi_6\equiv\tau_{0\bar{1}\cdot 01}$ and noting that $(\vec{K}_{0\bar{1}}-\vec{K}_{\bar{1}0})=(\vec{K}_{01}-\vec{K}_{10})$ and $(\vec{K}_{01}-\vec{K}_{\bar{1}0})=(\vec{K}_{0\bar{1}}-\vec{K}_{10})$, we can write the intensity pattern in the photoresist as

$$\begin{aligned}I(\vec{r})=I_0+2\{&c_1\cos[\vec{K}_{10}\cdot\vec{r}+\phi_1]+c_1\cos[\vec{K}_{\bar{1}0}\cdot\vec{r}+\phi_1]\\&+c_2\cos[\vec{K}_{01}\cdot\vec{r}+\phi_2]+c_2\cos[\vec{K}_{0\bar{1}}\cdot\vec{r}+\phi_2]\\&+2c_3\cos\phi_3\cos[(\vec{K}_{01}-\vec{K}_{10})\cdot\vec{r}]\\&+2c_4\cos\phi_4\cos[(\vec{K}_{0\bar{1}}-\vec{K}_{\bar{1}0})\cdot\vec{r}]+c_5\cos[(\vec{K}_{10}-\vec{K}_{\bar{1}0})\cdot\vec{r}\\&+\phi_5]+c_6\cos[(\vec{K}_{01}-\vec{K}_{0\bar{1}})\cdot\vec{r}+\phi_6]\}.\end{aligned} \tag{14}$$

It has been previously shown [46] that structures with large PBG's can be created by intensity patterns of the form

$$I(\vec{r})=I_0+C\{\cos(\vec{K}_{10}\cdot\vec{r})+\cos(\vec{K}_{\bar{1}0}\cdot\vec{r})+\cos(\vec{K}_{01}\cdot\vec{r})-\cos(\vec{K}_{0\bar{1}}\cdot\vec{r})\}, \tag{15}$$

where C is a real number.[1] In order to write Eq. (14) in this form, we make another translation $\vec{r}\rightarrow\vec{r}-\vec{\delta}_2$, such that $\vec{\delta}_2$ satisfies $\vec{K}_{10}\cdot\vec{\delta}_2=\phi_1$, $\vec{K}_{\bar{1}0}\cdot\vec{\delta}_2=\phi_1$, and $\vec{K}_{01}\cdot\vec{\delta}_2=\phi_2$. It is easy to verify that the translation $\vec{\delta}_2=(0,(\phi_2-\phi_1)a/2\pi,\phi_1 c/2\pi)$ provides the above properties. Under this change of coordinates, the intensity pattern becomes

[1] In Ref. [46] the vectors are written in terms of a different coordinate system.

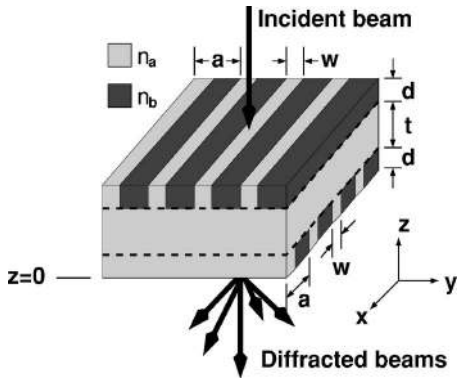

FIG. 1. Schematic representation of a three-layer phase mask. The top and bottom layers are orthogonally oriented binary gratings, and the middle layer is a homogeneous slab.

$$
\begin{aligned}
I(\vec{r}) = I_0 + 2\{&c_1\cos[\vec{K}_{10}\cdot\vec{r}] + c_1\cos[\vec{K}_{\bar{1}0}\cdot\vec{r}] \\
&+ c_2\cos[\vec{K}_{01}\cdot\vec{r}] + c_2\cos[\vec{K}_{0\bar{1}}\cdot\vec{r} + 2(\phi_2 - \phi_1)] \\
&+ 2c_3\cos\phi_3\cos[(\vec{K}_{01} - \vec{K}_{10})\cdot\vec{r} + (\phi_1 - \phi_2)] \\
&+ 2c_4\cos\phi_4\cos[(\vec{K}_{0\bar{1}} - \vec{K}_{\bar{1}0})\cdot\vec{r} - (\phi_1 - \phi_2)] \\
&+ c_5\cos[(\vec{K}_{10} - \vec{K}_{\bar{1}0})\cdot\vec{r} + \phi_5] + c_6\cos[(\vec{K}_{01} - \vec{K}_{0\bar{1}})\cdot\vec{r} \\
&+ \phi_6 + 2(\phi_1 - \phi_2)]\}. \qquad (16)
\end{aligned}
$$

Finally, in order to achieve an intensity pattern corresponding to Eq. (15), we desire to find a phase mask which produces modes whose corresponding **E** fields satisfy

$$
\begin{aligned}
&c_1 = c_2, \\
&\phi_2 - \phi_1 = \pm\frac{\pi}{2}, \quad \mathrm{mod}\ 2\pi, \\
&2c_j\cos\phi_j = 0, \quad j = 3,4, \\
&c_5 = c_6 = 0. \qquad (17)
\end{aligned}
$$

Equation (17) provides a target pattern against which actual intensity patterns from various phase masks can be evaluated. For a given intensity pattern, we search for the largest achievable PBG by calculating the photonic bands for structures whose solid-air boundaries are defined by several isointensity surfaces of the pattern. The optimal intensity threshold is then defined as one whose isointensity surface yields the largest PBG when the developed photoresist is replaced with silicon. However, by comparing the coefficients of intensity patterns to those in Eq. (17), one can save computational effort by discarding those intensity patterns which differ greatly from the target intensity pattern.

III. OPTICAL-PHASE-MASK ARCHITECTURE

We demonstrate the ability of a three-layer phase mask, as shown in Fig. 1, to achieve the target intensity pattern described in Sec. II. The phase mask consists of two identical, orthogonally arranged, one-dimensional binary gratings separated by a homogeneous slab of thickness t with refractive index n_a. The motivation for choosing such a design comes from its simplicity and its flexibility through variation of design to deliver target diffraction patterns.

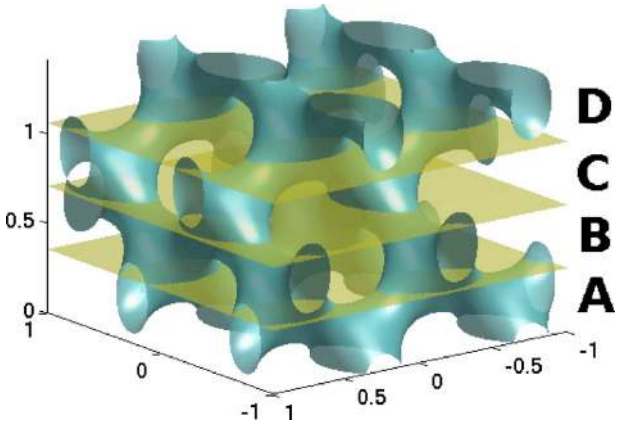

FIG. 2. (Color online) Four unit cells (one unit cell in the vertical direction) of an isointensity surface in the target intensity pattern, $I(\vec{r}) = I_0 + C\{\cos(\vec{K}_{10}\cdot\vec{r}) + \cos(\vec{K}_{\bar{1}0}\cdot\vec{r}) + \cos(\vec{K}_{01}\cdot\vec{r}) - \cos(\vec{K}_{0\bar{1}}\cdot\vec{r})\}$. The three planes indicate positions at $c/4$, $2c/4$, and $3c/4$ along the tetragonal direction.

The ideal intensity pattern described by Eqs. (16) and (17), shown in Fig. 2, consists of four repeating intensity slices along the tetragonal direction of the unit cell. This is characteristic of diamondlike structures. The four slices are labeled as A, B, C, and D in Fig. 2. Slices A and C differ by an in-plane translation, and slices B and D are a 90° rotation from slices A and C. In a very crude picture, the top layer of the proposed phase mask can be thought of as creating a two-dimensional diffraction pattern which generates the A and C slices of the desired shape, while the bottom layer generates a similar diffraction pattern that is rotated by 90° and translated in the vertical direction. The homogeneous OPM layer separating the binary gratings is introduced as a mechanism to control the translation between the diffraction patterns created by the two orthogonal, one-dimensional gratings so that the spacing between the slices A, B, C, and D is appropriate. However, this simple picture provides only a rough guide to the overall diffraction pattern. It does not account for the effects of reflections at layer boundaries and interference between the two orthogonal diffraction patterns of the separated grating layers of the OPM. Therefore the true intensity pattern must be calculated carefully.

Here, the diffraction-interference pattern created by the phase mask is calculated using the Fourier modal method [47] on a 1024×1024 grid and truncation order 441. In each layer of the OPM and in the homogeneous regions above and below, the electromagnetic field is expanded in terms of modes whose wave-vector x and y components correspond to the Fourier components of the OPM dielectric profile in the xy plane. In regions that are homogeneous in x and y, the z component of the wave vector of each mode is given by Eq. (1). In regions where the dielectric profile is periodic in the xy plane, the z component of the wave vector is calculated by Fourier expansion of the field in Maxwell's equations. The

resulting diffraction-interference pattern is obtained by matching boundary conditions at the interfaces between the layers. Photonic band structures are calculated with the plane-wave expansion method [6] using over 1440 plane waves, while Fourier coefficients of the dielectric structure are calculated using a discrete Fourier transform with 512 points per direction.

The binary grating layers of the phase mask, each of thickness d, consist of alternating regions of refractive index n_a and n_b with periodicity a. The n_a regions have width w and the n_b regions have width $(a-w)$. We characterize a given phase mask geometry by the set of adjustable parameters $[w,d,t]$. All lengths are expressed in units of a, the lattice constant of the phase mask and of the resulting photonic crystal. For concreteness, the refractive indices of the regions above the phase mask (from which the incident beam is launched) and below the phase mask (the region to be exposed) are $n^{(+)}=1$, corresponding to air, and $n^{(-)}=1.67$, corresponding to undeveloped SU-8 [45], respectively. We restrict our discussions to configurations that produce an intensity pattern with an aspect ratio $c/a=\sqrt{2}$, corresponding to a fcc Bravais lattice. This ratio has been shown [46] to maximize the PBG. Accordingly, we take the vacuum wavelength of the incident beam to be $\lambda_0=(2\sqrt{2}n^{(-)}a)/3$. The polarization vector of the incident beam is characterized by

$$\vec{E}_{\text{inc}} = \cos(\psi)\hat{x} - e^{i\chi}\sin(\psi)\hat{y}, \tag{18}$$

where $\hat{x}$ and $\hat{y}$ are unit vectors in the x and y directions, respectively, ψ is the linear polarization angle from $\hat{x}$ as measured looking along the incident beam, and χ is an "ellipticity" angle which indicates the phase delay between the x and y polarization components. In order to simplify the problem, we choose a linearly polarized incident beam ($\chi=0$). The symmetry of the target diamond structure suggests that we choose $\psi=45°$, so that the diffracted beams in the x and y directions have equal intensities. Intensities are given in units of the incident beam intensity.

IV. PHOTONIC BAND-GAP ARCHITECTURES

A. Direct structures

We first discuss photonic crystal structures consisting of solid material in the regions of high light intensities (above the threshold of the photoresist) and air in the regions of low light intensity (below the threshold). This, for example, corresponds to the case when a double-inversion process [5] is used with a negative photoresist or a single-inversion process is used with a positive photoresist. For illustration, we consider the case in which the grooves of the phase mask consist of air, so that $n_b=1$.

Figure 3 shows an iso-intensity surface in the interference pattern created by a phase mask with $[w,d,t]=[0.50,0.50,0.90]$ and $n_a=2.00$. The diamondlike characteristics of the interference pattern are apparent in the dielectric "nodes" connected to their nearest neighbors by tetrahedral "bonds." The five beams created in the photoresist by illumination of the phase mask from above have the wave vectors given in Eq. (2). The polarization vectors of these beams

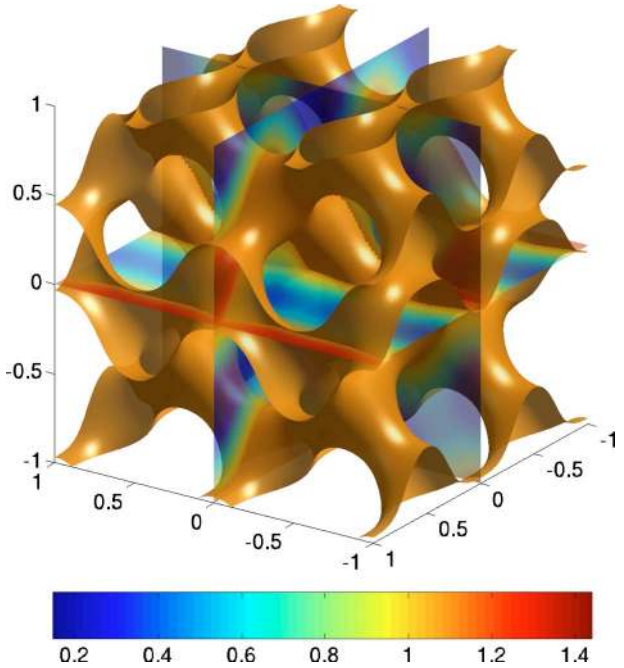

FIG. 3. (Color online) The isointensity surface at $I_{\text{thr}}=1.10$ in the intensity pattern created by a phase mask with $[w,d,t]=[0.50,0.50,0.90]$, $n_a=2.00$, and $n_b=1$. The volume fraction of the region inside the surface is ≈24%. When the high-intensity regions are replicated with silicon in an air background, the resulting structure displays a 24% 3D PBG.

are determined by the Fourier modal method and are given by

$$\vec{E}_{00} = (0.176 + i0.283, -0.145 - i0.303, 0),$$

$$\vec{E}_{10} = (-0.110 + i0.002, 0.218 - i0.147, -0.310 + i0.004),$$

$$\vec{E}_{\bar{1}0} = (-0.110 + i0.002, 0.218 - i0.147, 0.310 - i0.004),$$

$$\vec{E}_{01} = (0.129 + i0.202, -0.004 - i0.083, -0.011 - i0.235),$$

$$\vec{E}_{0\bar{1}} = (0.129 + i0.202, -0.004 - i0.083, 0.011 + i0.235). \tag{19}$$

The symmetry of the intensity pattern, Eq. (19), compares favorably with the target symmetry in Eq. (17). Quantitatively,

$$[c_1, c_2, \cos(\phi_1 - \phi_2), 2c_3\cos\phi_3, 2c_4\cos\phi_4, c_5, c_6] = [0.119, 0.106, 0.044, 0.000, 0.010, 0.015, 0.009]. \tag{20}$$

High-quality materials synthesis requires that the contrast in the optical diffraction pattern, between the highest-light-intensity regions and the lowest-light-intensity regions, be maximum. This makes the process less vulnerable to random fluctuations causing unwanted disorder in the developed photoresist. A dynamic range of the intensity pattern which is the

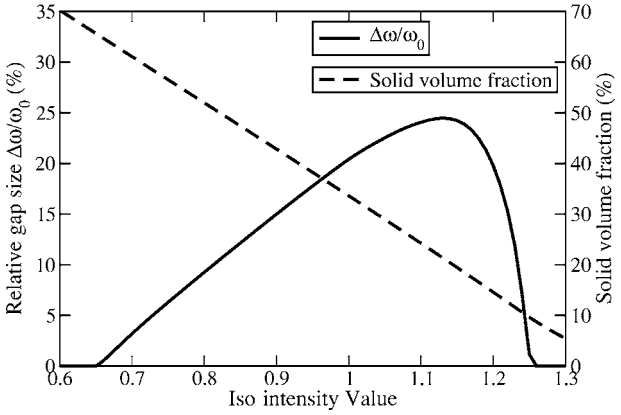

FIG. 4. Plot of the solid volume fraction and the relative PBG as functions of the threshold iso-intensity for photopolymerization, for the intensity pattern in Fig. 3. The high-intensity regions are assumed to map to a dielectric constant of 11.9 (corresponding to silicon) while the low-intensity regions correspond to air.

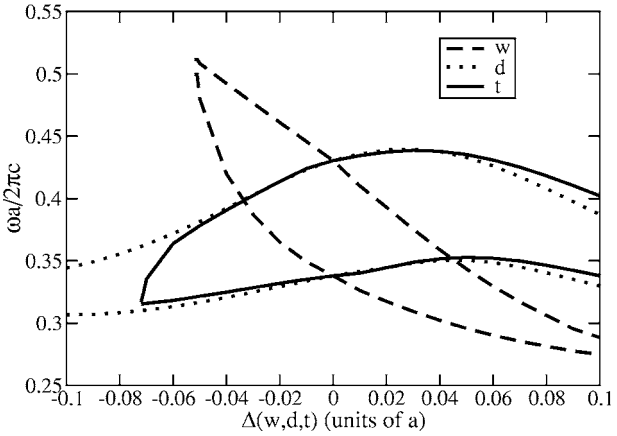

FIG. 6. The photonic band edges as functions of the change in the geometry of the phase mask. The deviation is measured a difference from a phase mask with $[w,d,t]=[0.50,0.50,0.90]$. The photopolymerization intensity threshold is held constant, and the structure is characterized by a 11.9:1 dielectric contrast.

largest possible fraction of the background intensity I_0 leads to the most effective exposure and development of the photoresist. Accordingly, we define the intensity contrast as

$$C \equiv (I_{\max} - I_{\min})/(2I_0). \tag{21}$$

The intensity pattern in Fig. 3 has a background intensity $I_0=0.818$, calculated from the polarization vectors according to Eq. (8), and reaches a minimum value $I_{\min}=0.204$ and a maximum value $I_{\max}=1.500$. The intensity contrast is therefore $C=0.762$. For comparison, the maximum intensity contrast that can be achieved using counterpropagating four-beam interference lithography to generate a diamondlike photonic crystal is 0.816 when elliptical polarizations are allowed and 0.472 when only linear polarizations are used [46].

Figure 4 shows the solid volume fraction and the PBG of the silicon replica of the developed photoresist (with a corresponding dielectric constant of 11.9) as functions of the threshold isointensity I_{thr} for photopolymerization. The mapping of the percentage volume fraction f to the isointensity value can be approximated as $f=-93I_{\text{thr}}+126$. The optimized structure has a solid volume fraction of 24% and yields a 3D PBG of spectral width $\Delta\omega/\omega_0=24\%$.

The photonic band structure corresponding to the optimized structure is shown in Fig. 5. The 3D PBG opens between bands 4 and 5, and is centered at $a/\lambda_0=0.38$. The gap is bounded on the upper edge at the R point and on the lower edge somewhere on the Γ-X segment.

It is important to consider the robustness and sensitivity of the PBG to changes in the structural phase mask parameters. The lattice constant of the phase mask grooves is equal to the lattice constant of the photonic crystal in the xy plane. It follows that to produce a structure with a PBG in the optical regime, the phase mask must have submicron features. Typically, a 3D PBG centered at 1.5 μm made from a silicon photonic crystal requires a lattice constant $a \simeq 600$ nm.

Figure 6 shows the change in the photonic band-gap edges of the resulting structure when the phase mask geometry deviates from $[w,d,t]=[0.50,0.50,0.90]$, for a fixed

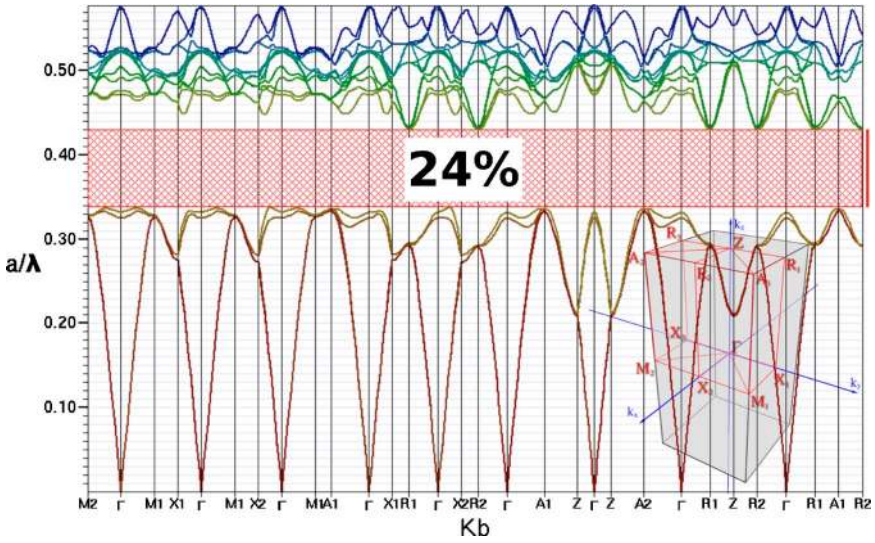

FIG. 5. (Color online) Photonic band structure diagram for the optimized structure created by the intensity pattern in Fig. 3 characterized by 11.9:1 dielectric contrast. The inset shows the positions of the high-symmetry points in the reciprocal lattice. A 3D PBG of width $\Delta\omega/\omega_0=24\%$ opens between bands 4 and 5.

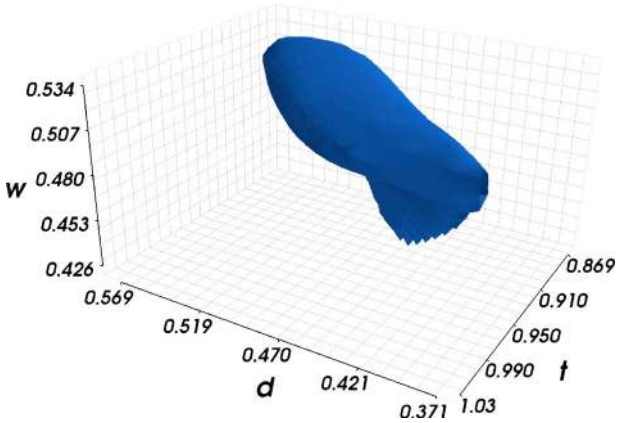

FIG. 7. (Color online) Isosurface plot of the magnitude of the PBG in three-dimensional space of $[w,d,t]$ for a direct silicon OPML photonic crystal created from a phase mask with $n_a=2.0$. The isosurface corresponds to a gap size of $\Delta\omega/\omega_0=20\%$. The relative PBG is larger than 20% inside the volume.

value of the photopolymerization intensity threshold. For small deviations in d and in t the effects are similar, since both cause changes in the path length of light passing through the phase mask. However, changes in d have the additional effect of changing the strength of the diffraction by the phase mask. Therefore, at larger deviations, the effect of a change in d differs from that of a change in t.

Figure 7 shows an isosurface plot of the magnitude of the PBG in three-dimensional space of $[w,d,t]$, for a direct silicon structure created from a phase mask with $n_a=2.0$. The isosurface shown in Fig. 7 corresponds to a gap size $\Delta\omega/\omega_0=20\%$. Regions inside the depicted surface represent structures with PBGs larger than 20% relative to the gap center frequency. At constant values of the groove width w, when each grating thickness d is increased, the grating separation t must be decreased in order for the geometry to remain in the large PBG region. The size of the PBG tends to be more sensitive to changes in t than in d and w. The minimum sensitivity to t is reached for values of w between 0.50 and 0.55.

The variation of the intensity pattern (and PBG of the resulting structure) with changes in the incident beam characteristics is also of importance. Although we do not make use of the incident beam as a design parameter here, it is worthwhile, for practical purposes, to know the robustness of the diffraction-interference pattern (and resulting PBG) against deviations in the incident beam parameters.

First, we consider the effect of changing the linear polarization angle ψ on the relative PBG size and band-edge positions. The results are shown in Fig. 8. The relative PBG magnitude remains above 10% over a change in ψ of ±5°.

Removing the linear polarization restriction on the incident beam provides further design flexibility by allowing the ellipticity angle χ in Eq. (18) to vary. For illustration, we consider a simple path in the two-dimensional polarization parameter space by fixing $\psi=45°$ and allowing χ to vary. Figure 9 shows the relative PBG size and band edge positions as χ is varied from 0° (corresponding to the linear polarization) to ±90° (corresponding to two orthogonal circular polarizations). The PBG does not close at any value of χ, although the relative PBG size drops to just above 10% when the incident beam is circularly polarized. This indicates that the intensity pattern is more dependent on the relative amplitudes of the polarization vector components in the $\hat{x}$ and $\hat{y}$ directions than on the relative phase between the two components.

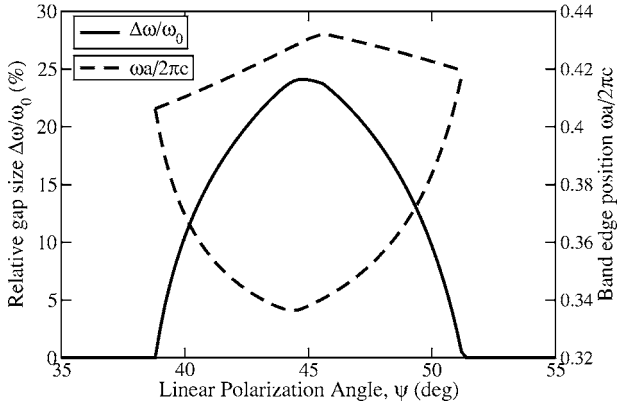

FIG. 8. The relative PBG size and band-edge positions as functions of the linear polarization angle ψ of the incident beam. The beam passes through a phase mask with geometry $[w,d,t]=[0.50,0.50,0.90]$, and the resulting intensity pattern is synthesized with a 11.9:1 dielectric contrast at a photopolymerization intensity threshold of 1.10. The PBG magnitude remains above 10% over a change in ψ of ±5°.

The refractive index of the phase mask is a particularly important design consideration.

Figure 10 shows the PBG size in $[w,d,t]$ space with groove width $w=0.50$, using different phase masks with refractive indices of $n_a=1.95$, $n_a=2.00$, and $n_a=2.05$. For each of the refractive indices, we identify regions in the $[d,t]$ parameter space where structures with large PBG's can be generated upon replication with silicon. As one decreases the refractive index of the phase mask from $n_a=2.00$ to n_a

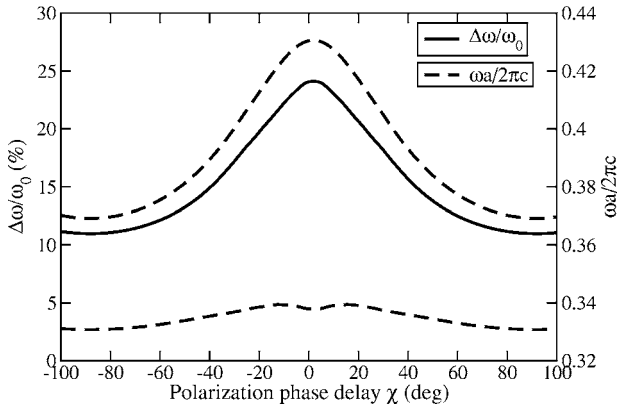

FIG. 9. The relative PBG size and band-edge positions as functions of the incident beam polarization "ellipticity" χ for structures created using a phase mask with geometry $[w,d,t]=[0.50,0.50,0.90]$ and synthesized with a material with dielectric constant 11.9. When $\chi=0°$, the incident beam is linearly polarized, with linear polarization angle $\psi=45°$, while at $\chi=\pm90°$, the incident beam is circularly polarized.

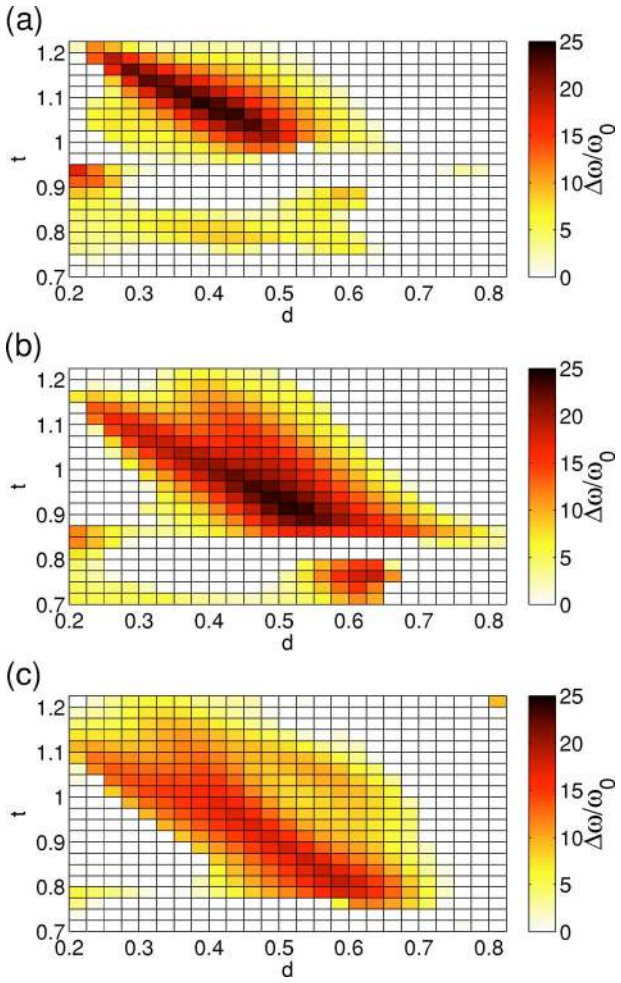

FIG. 10. (Color online) The relative PBG size of structures created by different phase masks with refractive indices (a) $n_a=1.95$, (b) $n_a=2.00$, and (c) $n_a=2.05$ in $[w,d,t]$ space with groove width $w=0.50$. The shade in a rectangle corresponds to the PBG size at the value of the grating depth d and separator layer thickness t at the lower left corner of the rectangle, according to the bar on the right. The photopolymerization intensity threshold is set at a value of 1.10. Regions exposed to intensities above the threshold are replicated with a material with dielectric constant 11.9.

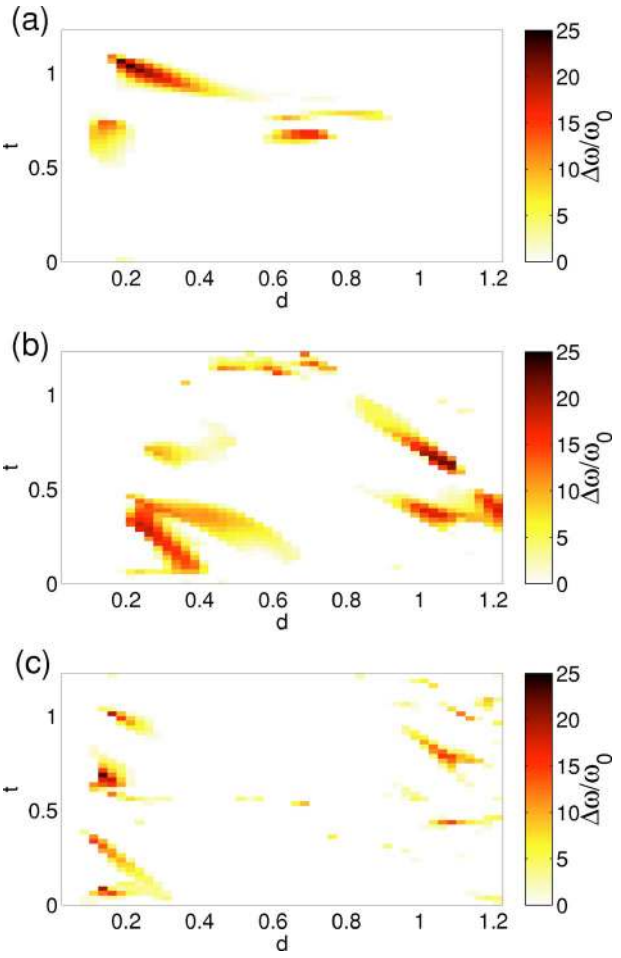

FIG. 11. (Color online) PBG size of structures created by phase masks with refractive indices (a) $n_a=1.7$, (b) $n_a=2.3$, and (c) $n_a=2.5$, with groove width $w=0.50$, and various values of grating depth d and separator thickness t. The corresponding photopolymerization threshold intensities are (a) $I_{\text{thr}}=0.78$, (b) $I_{\text{thr}}=1.37$, and (c) $I_{\text{thr}}=0.93$. Regions exposed to intensities larger than I_{thr} are replicated with silicon (dielectric constant 11.9). The shade of a rectangle in the figure corresponds to the PBG size resulting from a phase mask with values of d and t at the lower left corner of the rectangle (the rectangle edges are omitted for clarity).

$=1.95$, a shallower grating depth d and larger separator layer thickness t are required to compensate and produce structures with large PBG's. On the other hand, as the refractive index is increased from $n_a=2.00$ to $n_a=2.05$, not only does the large-PBG region move to larger groove depth d and smaller grating separation t, but the maximum PBG size also drops to about 18%. It is important to note that for high refractive indices, even with small changes in the refractive index of the phase mask, the size of the PBG can vary greatly—for example, a phase mask geometry with $d=0.50$, $t=0.90$, and $n_a=2.0$, which produces a structure with a 24% PBG at $I_{\text{thr}}=1.10$. The same mask structure produces only a 15% PBG for $n_a=2.05$ and does not even produce a PBG when $n_a=1.95$. It is therefore important to choose phase mask structure according to the particular composition of the mask.

It is of considerable importance to define an ideal range of refractive index contrasts for the optical phase mask. This is governed by a trade-off between high intensity contrast in the interference-diffraction pattern and robustness of the optical interference pattern to random perturbations in the OPM architecture. Both of these factors are important for the development of high-quality PBG materials with minimal disorder.

Figure 11 shows the relative gap size of structures resulting from phase masks with groove width $w=0.50$ and refractive indices $n_a=1.7$, $n_a=2.3$, and $n_a=2.5$, with corresponding threshold intensities $I_{\text{thr}}=0.78$, $I_{\text{thr}}=1.37$, and $I_{\text{thr}}=0.93$. When $n_a=1.7$ and $n_a=2.3$, there are large-PBG regions in $[w,d,t]$ space, comparable in size to the regions shown for $n_a=2.0$ in Fig. 10. However, when the refractive index of the phase mask increases to $n_a=2.5$, the large-PBG regions in the $[w,d,t]$ space shrink considerably. This implies that the interference-diffraction pattern is very sensitive to small perturbations in the phase mask structure. For phase masks with

n_a greater than 2.5, this undesirable sensitivity worsens and large-PBG regions in $[w,d,t]$ space are no longer robust to manufacturing error in the OPM. On the other hand, when the refractive index of the phase mask is decreased below $n_a=1.7$, the intensity contrast of the resulting interference pattern is lowered. This in turn makes the photonic crystal architecture more susceptible to disorder arising from inhomogeneities in the photoresist and small random variations in the photopolymerization threshold.

B. Inverse structures

In the previous section, we considered photonic band-gap architectures that were high-refractive-index replicas of the optical diffraction-interference pattern where the optical intensity exceeds a prescribed threshold value. Such "direct structures" could be made by silicon double inversion [5] of an SU-8 polymer photoresist exposed by the optical interference pattern or by a single step in certain chalcogenide glasses that are amenable to direct photopolymerization [48]. On the other hand, the situation may arise wherein the final photonic crystal structure will be defined by high-refractive-index material in the low-intensity regions of OPML and consist of air in the high-intensity regions of the OPM diffraction-interference pattern. We refer to these as "inverse structures." For example, use of a negative photoresist and a single-inversion process or a positive photoresist and a double-inversion process will yield such results. For the target intensity pattern described in Eq. (16) with the coefficients given in Eq. (17), the equivalent but inverted structure (solid and air regions interchanged) is defined by the isointensity value I_{thr} obtained by the "transformation" $I_{\text{thr}} \rightarrow -I_{\text{thr}}+2I_0$ [to within a translation of $(a/2,a/2,c)$]: Consider the shape functions S_d of the direct structure and S_i of the inverted structure, defined by

$$S_d(\vec{r},I_{\text{thr}}) = \Theta(I(\vec{r}) - I_{\text{thr}}),$$

$$S_i(\vec{r},I_{\text{thr}}) = \Theta(I_{\text{thr}} - I(\vec{r})). \tag{22}$$

Here $\Theta(x)$ is the Heaviside step function [$\Theta(x)=1$ for $x \geq 0$ and 0 otherwise]. When $I(\vec{r})$ corresponds to the idealized, target intensity pattern in Eq. (16) with coefficients Eq. (17), taking $\vec{r}'=\vec{r}-(a/2,a/2,c)$ implies $I(\vec{r}')=-I(\vec{r})+2I_0$. We can therefore write

$$S_i(\vec{r}',-I_{\text{thr}}+2I_0) = \Theta(-I_{\text{thr}}+I(\vec{r})) = S_d(\vec{r},I_{\text{thr}}). \tag{23}$$

For this specific, idealized intensity pattern, the PBG structure can be achieved using either fabrication algorithm, yielding solid material in high-intensity regions (direct structure) or yielding solid material in the "transformed" low-intensity regions (inverse structure). However, this equivalence is specific to the idealized, target intensity. When the coefficients in the intensity pattern do not match the targets in Eq. (17), then there is no simple "transformation" to equivalent but inverted structures at different intensity thresholds. Since OPML intensity patterns in this paper differ slightly from the idealized, target pattern [see Eq. (20)], it is necessary to consider separately the case of "inverse structures."

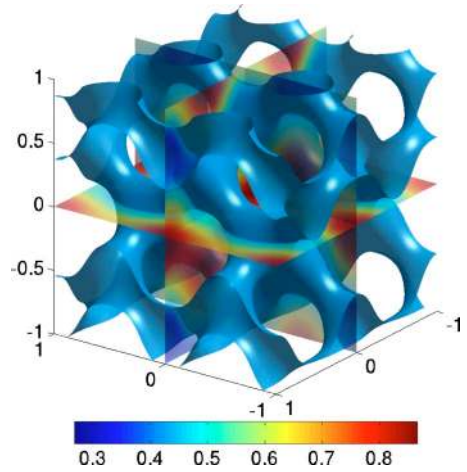

FIG. 12. (Color online) The isointensity surface at photopolymerization intensity threshold $I_{\text{thr}}=0.43$ in the intensity pattern generated by a phase mask with $[w,d,t]=[0.50,0.10,0.50]$, $n_a=2.0$, and $n_b=1.0$. The volume fraction of the region inside the surface is $\approx 22\%$. When the low-intensity regions (regions inside the surface) are replicated with a material with dielectric constant 11.9 in an air background, the resulting structure displays a 24% 3D PBG.

With the understanding that the actual OPML intensity pattern differs slightly from the target pattern, we revisit the phase mask with $[w,d,t]=[0.50,0.50,0.90]$ and $n_a=2.0$. Application of the algorithm $I_{\text{thr}} \rightarrow -I_{\text{thr}}+2I_0$ with initial threshold $I_{\text{thr}}=1.10$ and I_0 calculated from Eq. (19) yields a transformed threshold intensity $I_{\text{thr}}=0.54$. When the regions illuminated by intensities lower than the threshold value are infiltrated by a solid with dielectric constant 11.9, the resulting structure displays an 18% PBG at a solid volume fraction of $\approx 24\%$. Adjusting the intensity threshold to $I_{\text{thr}}=0.58$ produces a structure with a 19% PBG, several percent smaller than the case where the overexposed regions consist of the same solid material.

While the phase mask with geometry $[w,d,t]=[0.50,0.50,0.90]$ is better suited to "direct" PBG architectures, other phase mask geometries exist for which the opposite is true. For example, a phase mask with geometry $[w,d,t]=[0.50,0.10,0.50]$ generates the diffraction-interference pattern shown in Fig. 12, with an intensity contrast $C=0.53$. This leads to a structure with a 24% PBG after Si infiltration of the regions with light intensity below $I_{\text{thr}}=0.43$ in the template. On the other hand, the "direct" silicon structure (filling high-intensity regions) yields, at best, only a 21% PBG when the threshold intensity is optimized to $I_{\text{thr}}=0.70$.

Figure 13 shows the PBG map of "inverse structures" created by phase masks with $w=0.50$ and various values of d and t. Here, the phase mask index of refraction is $n_a=2.00$ and the photopolymerization intensity threshold is $I_{\text{thr}}=0.43$. There are several geometries in the region surrounding $[w,d,t]=[0.50,0.10,0.50]$ which yield "inverse structures" exhibiting a large PBG. The other large-PBG regions in the figure point to the possibility of generating large-PBG structures with other phase mask geometries. For each particular region, the actual PBG can be made larger than those shown in Fig. 13 when I_{thr} is further optimized.

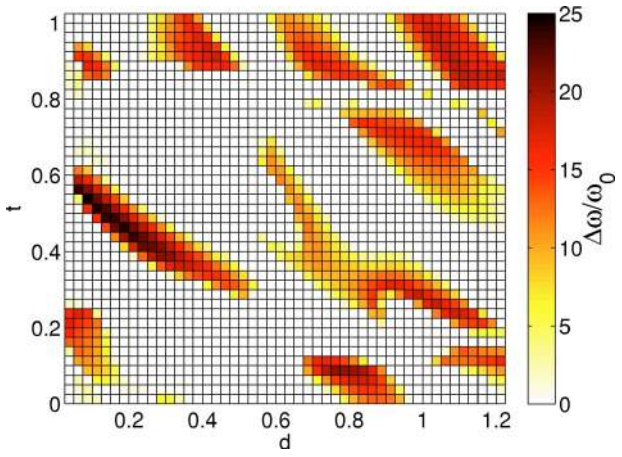

FIG. 13. (Color online) PBG size of structures created by phase masks with groove width $w=0.50$ and grating depth d and grating separation t varying. The refractive index of the phase mask is $n_a=2.0$ and the photopolymerization intensity threshold is set at $I_{\text{thr}}=0.43$. Regions exposed to intensities below I_{thr} are replicated with a material with dielectric constant 11.9. The shade of a rectangle displays, according to the colorbar to the right, the PBG resulting from a phase mask with d and t corresponding to the values at the lower left corner of the rectangle.

V. CONCLUSIONS

We have shown that single-exposure, optical-phase-mask lithography based on diffraction and interference patterns from a single beam normally incident on suitably designed phase masks can be used to create diamondlike photonic crystals with large PBG's. The phase mask design was facilitated by introducing a target five-beam interference pattern in an umbrella configuration, identical to the four-beam counterpropagating interference pattern proposed previously for generating a diamondlike photonic crystal [46]. Using the OPM to generate five interfering beams from a single incident beam places the role of controlling the relative phases, polarizations, amplitudes, and wave vectors of the interfering beams on the phase mask itself. Unlike multibeam holographic lithography [32,37], in OPML only the parameters of the single incident beam need to be precisely controlled. The relative PBG sizes of final silicon-based "direct" structures remain over 10% even when the linear polarization angle changes by ±5°. Since the OPML intensity pattern is determined by the design of the phase mask, it is only possible to realize a close approximation to the target intensity pattern of more general five-beam interference. The resulting reduction of symmetry in the OPML pattern, however, leads only to a slight decrease in the PBG size (from 25% to 24% in the cases discussed here). The reduction in symmetry also leads to a distinction between "direct" and "inverse" photonic crystal architectures. We have investigated phase mask geometries for the situation when the incident beam enters the mask from air ($n^{(+)}=1$) and the resulting interference pattern illuminates a region below the mask with dielectric constant $n^{(-)}=1.67$. We have demonstrated OPM geometries for phase masks with refractive indices n_a varying between 1.7 and 2.3 that produce intensity patterns to yield a variety of photonic crystal structures with large PBG's. The intensity contrast in OPML is comparable to that which can be achieved using counterpropagating four-beam holography. The optimal phase mask geometry is sensitive to the refractive indices of the phase mask and the photoresist. Therefore, the phase mask structure must be tailored specifically to the chosen constituent materials. Moreover, there may be several regions in the parameter space of phase mask geometries that can produce a suitable intensity pattern. We provided an illustration of a robust geometry, suitable to fabricate a "direct" silicon PBG material. The PBG in this "direct" silicon structure persists despite 8% variations in the thickness of the homogeneous middle layer of the phase mask and despite more than a 10% variation in either the width or thickness of the phase mask grooves. Our paper provides illustrative examples of OPML with specific, simple choices of phase masks. By expanding the parameter space of the phase mask design, other blueprints for fabricating photonic crystals by single-exposure phase mask lithography may be found. For instance, the depth of the two binary gratings (woodpile layers) can be allowed to vary independently. Also, the regions between the grooves of the phase mask can be infiltrated by a material with refractive index n_b, to allow for further flexibility in the phase mask design.

The fabrication of the phase mask itself may require high precision lithographic processes widely used for two-dimensional microstructures. The lattice constant of the phase mask grooves equals the lattice constant of the resulting photonic crystal itself, with corresponding submicron feature sizes. However, after the phase mask is fabricated, it can be used repeatedly to expose many photoresists and for the simple and efficient mass production of 3D PBG materials.

ACKNOWLEDGMENTS

This work was supported in part by the National Sciences and Engineering Research Council (NSERC) of Canada and the Ontario Premier's Platinum Research Prize for Science.

[1] Sajeev John, Phys. Rev. Lett. **58**, 2486 (1987).
[2] Eli Yablonovitch, Phys. Rev. Lett. **58**, 2059 (1987).
[3] Sajeev John, Phys. Rev. Lett. **53**, 2169 (1984).
[4] Alongkarn Chutinan, Sajeev John, and Ovidiu Toader, Phys. Rev. Lett. **90**, 123901 (2003).
[5] Nicolas Tétrault *et al.*, Adv. Mater. (Weinheim, Ger.) **18**, 457 (2006).
[6] K. M. Ho, C. T. Chan, and C. M. Soukoulis, Phys. Rev. Lett. **65**, 3152 (1990).
[7] H. S. Sözüer and J. P. Dowling, J. Mod. Opt. **41**, 231 (1994).

[8] C. T. Chan, K. M. Ho, C. M. Soukoulis, R. Biswas, and M. Sigalas, Solid State Commun. **89**, 413 (1994).
[9] S. Y. Lin *et al.*, Nature (London) **394**, 251 (1998).
[10] J. G. Fleming and Shawn-Yu Lin, Opt. Lett. **24**, 49 (1999).
[11] S. Noda, K. Tomoda, N. Yamamoto, and A. Chutinan, Science **289**, 604 (2000).
[12] Kanna Aoki, Hideki T. Miyazaki, Hideki Hirayama, Kyoji Inoshita, Toshihiko Baba, Norio Shinya, and Yoshinobu Aoyagi, Appl. Phys. Lett. **81**, 3122 (2002).
[13] Hong-Bo Sun, Shigeki Matsuo, and Hiroaki Misawa, Appl. Phys. Lett. **74**, 786 (1999).
[14] Brian H. Cumpston *et al.*, Nature (London) **398**, 51 (1999).
[15] Markus Deubel, Georg von Freymann, Martin Wegener, Suresh Pereira, Kurt Busch, and Costas M. Soukoulis, Nat. Mater. **3**, 444 (2004).
[16] Scott R. Kennedy, Michael J. Brett, Ovidiu Toader, and Sajeev John, Nano Lett. **2**, 59 (2002).
[17] Ovidiu Toader and Sajeev John, Science **292**, 1133 (2001).
[18] Ovidiu Toader and Sajeev John, Phys. Rev. E **66**, 016610 (2002).
[19] Scott R. Kennedy *et al.*, Photonics Nanostruct. Fundam. Appl. **1**, 37 (2003).
[20] E. Yablonovitch, T. J. Gmitter, and K. M. Leung, Phys. Rev. Lett. **67**, 2295 (1991).
[21] C. C. Cheng and A. Scherer, J. Vac. Sci. Technol. B **13**, 2696 (1995).
[22] C. C. Cheng, A. Scherer, V. Arbet-Engels, and E. Yablonovitch, J. Vac. Sci. Technol. B **14**, 4110 (1996).
[23] G. Feiertag *et al.*, Appl. Phys. Lett. **71**, 1441 (1997).
[24] A. Chelnokov, K. Wang, S. Rowson, P. Garoche, and J.-M. Lourtioz, Appl. Phys. Lett. **77**, 2943 (2000).
[25] Ovidiu Toader, Mona Berciu, and Sajeev John, Phys. Rev. Lett. **90**, 233901 (2003).
[26] H. Míguez, A. Blanco, F. Meseguer, C. López, H. M. Yates, M. E. Pemble, V. Fornés, and A. Mifsud, Phys. Rev. B **59**, 1563 (1999).
[27] A. Blanco *et al.*, Nature (London) **405**, 437 (2000).
[28] Yu. A. Vlasov, V. N. Astratov, A. V. Baryshev, A. A. Kaplyanskii, O. Z. Karimov, and M. F. Limonov, Phys. Rev. E **61**, 5784 (2000).
[29] Kurt Busch and Sajeev John, Phys. Rev. E **58**, 3896 (1998).
[30] Zhi-Yuan Li and Zhao-Qing Zhang, Phys. Rev. B **62**, 1516 (2000).
[31] V. Berger, O. Gauthier-Lafaye, and E. Costard, J. Appl. Phys. **82**, 60 (1997).
[32] M. Campbell *et al.*, Nature (London) **404**, 53 (2000).
[33] S. Shoji and S. Kawata, Appl. Phys. Lett. **76**, 2668 (2000).
[34] H. Miguez *et al.*, Chem. Commun. (Cambridge) 2736 (2002).
[35] Y. A. Vlasov, X.-Z. Bo, J. C. Sturm, and D. J. Norris, Nature (London) **414**, 289 (2001).
[36] Chaitanya K. Ullal *et al.*, J. Opt. Soc. Am. A **20**, 948 (2003).
[37] D. N. Sharp, A. J. Turberfield, and R. G. Denning, Phys. Rev. B **68**, 205102 (2003).
[38] Ovidiu Toader, Timothy Y. M. Chan, and Sajeev John, Phys. Rev. Lett. **92**, 043905 (2004).
[39] Xianyu Ao and Sailing He, Opt. Express **12**, 978 (2004).
[40] Chaitanya K. Ullal, Martin Maldovan, Edwin L. Thomas, Gang Chen, Yong-Jin Han, and Shu Yang, Appl. Phys. Lett. **84**, 5434 (2004).
[41] D. C. Meisel, M. Wegener, and K. Busch, Phys. Rev. B **70**, 165104 (2004).
[42] Seokwoo Jeon *et al.*, Proc. Natl. Acad. Sci. U.S.A. **101**, 12428 (2004).
[43] Y. Lin, P. R. Herman, and K. Darmawikarta, Appl. Phys. Lett. **86**, 071117 (2005).
[44] Y. Lin, P. R. Herman, and E. L. Abolghasemi, J. Appl. Phys. **97**, 096102 (2005).
[45] Yu. V. Miklyaev *et al.*, Appl. Phys. Lett. **82**, 1284 (2003).
[46] Timothy Y. M. Chan, Ovidiu Toader, and Sajeev John, Phys. Rev. E **71**, 046605 (2005).
[47] Lifeng Li, J. Opt. Soc. Am. A **14**, 2758 (1997).
[48] S. Wong, M. Deubel, F. Pérez-Willard, S. John, G. A. Ozin, M. Wegener, and G. von Freyman, Adv. Mater. (Weinheim, Ger.) **19**, 265 (2006).